Scaling laws for extremely strong thermals

Alex Skvortsov [1,*] Timothy C. DuBois [2] Milan Jamriska,[1] and Martin Kocan [1,†]
[1]*Defence Science and Technology Group, 506 Lorimer Street, Fishermans Bend, Victoria 3207, Australia*
[2]*Stockholm University, Stockholm SE-10691, Sweden*

(Received 25 September 2020; accepted 12 April 2021; published 3 May 2021)

A rich variety of scaling laws for the evolution of convective buoyant thermals generated by an explosive release of energy has been established. Such events may correspond to a blast, spark, or volcano eruption. It was found that an occurrence of a particular scaling law depends on the interplay of many factors, *viz.*, (1) amount of energy released in the environment, (2) time since the release, and (3) spatial scale of the release domain. The analytical treatment involves solutions of coupled equations for mass, momentum and buoyancy (heat) conservation in the Boussinesq and non-Boussinesq approximation. A model for the entrainment flow that accounts for a strong thermal flux has been proposed. For the limiting case of a weak thermal and the Boussinesq approximation (low density contrast between the buoyant thermal and the ambient environment) the celebrated Batchelor, Morton, and Turner scalings are recovered. Results have been favorably compared with limited data available in the literature.

DOI: 10.1103/PhysRevFluids.6.053501

I. INTRODUCTION

Convective plumes and thermals are ubiquitous environmental features that occur whenever an isolated density perturbation evolves driven by buoyancy and drag. Such thermals are usually associated with a rapid release of energy due to natural or anthropogenic events (volcano eruptions, solar corona activity, explosions, and industrial accidents; see [1–5] and references therein). Formally, the generation of thermals is one of the mechanisms which disperses and dissipates the energy imbalance. Convective thermals have extensively been investigated theoretically and experimentally, and there is a vast body of literature on this subject [1,6–10].

Since the seminal results of Batchelor, Morton, and Turner (BMT) [11–13] who laid foundations of the classical convective plume theory, it has been recognized that convective thermals exhibit remarkable scaling properties. These properties are a signature of the fact that the convective motion associated with the thermals is determined by only one parameter, *viz.*, the total energy released in the environment. Mathematically, these scaling properties manifest themselves as power laws for thermal evolution

$$Z \propto B_0^{\eta} t^{\gamma}, \quad R \propto B_0^{\theta} t^{\delta}, \tag{1}$$

where Z is the elevation of the centroid of the thermal from the source, R is the effective radius of the thermal, t is the time from the release, and B_0 is the so-called total buoyancy [proportional to the total energy released in the environment $E = \rho_r c_p B_0/(\alpha g)$, where ρ_r, c_p, and α are the density, specific heat, and thermal expansion coefficient of thermal's substance, respectively, and g is the

*Corresponding author: alex.skvortsov@dst.defence.gov.au
†Corresponding author: martin.kocan@dst.defence.gov.au

FIG. 1. A rising convective thermal after a nuclear explosion. Photo courtesy of the Los Alamos National Laboratory, U.S. Department of Energy [15].

gravity acceleration [14]]. The values of the power-law exponents are universal [11–13],

$$\gamma = \delta = 1/2, \quad \eta = \theta = 1/4, \tag{2}$$

and independent from other parameters.

Predictions from Eqs. (1) and (2) rest on two assumptions: (1) the Boussinesq approximation for convective flows (e.g. a small density contrast between the thermal and the ambient environment) and (2) an assumption for so-called entrainment velocity [16–18], which controls in-thermal flow fluxes:

$$v_e(t) = a\, w(t), \tag{3}$$

where $a = 0.1$–0.25 is an empirical constant and $w(t) = dZ/dt$ is the rising velocity of the thermal centroid [11–13].

The scaling from Eqs. (1) and (2) has been extensively verified experimentally, and within the validity of the Boussinesq approximation, a good agreement with the theory has been found; see [19,20] and references therein. Beyond the Boussinesq approximation, i.e., when the density contrast becomes significant, the agreement with prediction, Eq. (2), has become less convincing, and this necessitates an extension of the original BMT theory to overcome the limitations imposed by the Boussinesq approximation.

To incorporate non-Boussinesq effects and strong entrainment fluxes the original theory [11–13] has been modified [21–24]. One of the common modifications of the conventional model has been the replacement of the equation for entrainment velocity [Eq. (3)] with an expression that explicitly includes the density contrast (see [21,22] and references therein):

$$v_e(t) = a[\rho(t)/\rho_a]^{1/2} w(t), \tag{4}$$

where $\rho(t)$ is the density of the buoyant thermal and ρ_a is the density of the surrounding ambient medium.

In some cases this modification has improved the agreement with experiments, but overall (see [10] and references therein), the theory of non-Boussinesq plumes and thermals is far from completion and is still an area of active research [21,25,26].

Another line of research of similar phenomena is related to atmospheric sciences. It deals with the evolution of thermals as a possible mechanism of cloud formation [27,28]. In this case the thermal is modelled as a large-scale density anomaly and a small density contrast with the aim to predict its evolution. The weakness of the density contrast justifies the Boussinesq approximation, while

the large size of the thermal allows us to neglect the contribution of entrainment fluxes (which are proportional to the surface area and become insignificant in comparison with any volume effects, such as buoyancy).

As a result, the initial (buoyancy-dominated) stage of the thermal motion is reduced to the uniform updraft acceleration leading to a different value of scaling exponents than in Eq. (1): $\gamma \approx 2$, $\delta \approx 0$ [29]. As the thermal reaches its terminal velocity (when buoyancy is compensated by drag) the exponent γ reduces to $\gamma \approx 1$. It is worth noting that these values of γ are much higher than given by the BMT model, and this is a direct consequence of the thermal losing buoyancy via entrainment fluxes.

The subject of the presented study is somewhat extremely different from the original concept of the Boussinesq thermal. We assume an energy source that creates a thermal so powerful that the generated density contrast is of the same order of magnitude as the environmental density. In other words, due to thermal expansion, the initial density inside the thermal becomes relatively small (sometimes even negligible). Such a thermal can be conceptualized as a "hot cavity" or "bubble" that rises upwards driven by buoyancy and rapidly cools down. Figure 1 shows an image of a mushroom cloud formed by a nuclear detonation. The iconic mushroom cloud begins as a fireball, a luminous bubble of extremely hot air and vaporized weapon residues. The fireball rises like a hot-air balloon (hot cavity), pulling air, water vapor, and debris into its base to form the mushroom stem. As the fireball rises, it cools, losing its glow, and the vaporized material and water vapor condense and spread, forming the mushroom head [15,30].

The appropriate conditions for the formation of the strong thermal can be fulfilled in a strong blast, straight after the initial pressure disturbances equilibrate [31]. The created density and thermal anomaly will dissipate on a much longer timescale (driven by dissipation processes), so the evolution of such a thermal will initially follow the hot cavity model, switching to the Boussinesq regime at a much later stage. Conceptually, similar phenomena occur immediately after a rapid release of a large volume of air in deep water [32].

We propose a simple analytical theory for the evolution of such an "extremely" strong thermal. Our motivation for this theory stemmed from the analytical results for a convective flow generated by a point release of energy in an incompressible fluid (spherically symmetrical heat expansion). According to [33] this flow can be described by a self-similar solution that is amenable to analytical treatment. An important result of this study is the expression for entrainment velocity of the expanding buoyant thermal in terms of a heat flux

$$v_e(t) = \beta \frac{\partial T(r,t)}{\partial r}, \tag{5}$$

where $\beta \equiv \beta(T)$ is the thermal diffusivity (in general temperature-dependent), $T(r,t)$ is the distribution of temperature inside the buoyant thermal, r is the distance to the center of the thermal, which is assumed to be spherical (see below), and the gradient is taken at the surface of the thermal.

We emphasize that the expression for entrainment velocity, Eq. (5), is deduced from the analytical solution of fluid motion without any additional closure assumption. Straight after the rapid energy release, at the beginning of the cooling phase, the conventional entrainment fluxes are insignificant (since the vertical velocity of the thermal is small) and the evolution of the hot cavity is mostly driven by strong thermal fluxes and thermal-induced velocity. As a conceptual model we consider an initial profile of a hot cavity given by a spherically symmetric distribution of temperature, $T = T_0(r) = T_a + A_k(r/R_0)^{-k}$ at $t = 0$ and $\partial T(r)/\partial r = 0$ at $r = 0$, where T_a is the ambient temperature, R_0 is the initial radius of the buoyant thermal at the initial time $t = 0$, and A_k and k are positive constants. By discarding the effect of buoyancy from the shape of the cavity, further evolution of the system can be described by the three equations for an isobaric, spherically symmetric heat

conduction process in a moving gas (see [33] and references therein):

$$\frac{\partial \rho}{\partial t} + \frac{1}{r^2}\frac{\partial}{\partial r}(r^2 \rho V_r) = 0, \tag{6}$$

$$\rho c_p \left(\frac{\partial T}{\partial t} + V_r \frac{\partial T}{\partial r} \right) = \frac{1}{r^2}\frac{\partial}{\partial r}\left(\kappa r^2 \frac{\partial T}{\partial r} \right), \tag{7}$$

$$\rho T = \rho_0 T_0 = \rho_a T_a = \text{const}, \tag{8}$$

where T_0 and ρ_0 are the initial values of the temperature and density of the buoyant thermal at $t = 0$, respectively, V_r is the velocity of the gas, and $\kappa = \kappa(T)$ is the temperature-dependent heat conductivity. An important insight into the analytical solutions of these equations comes from the observation that if we assume $V_r = v_e$, Eq. (5), in the right-hand side of Eq. (7), then, after substituting $\rho \propto 1/T$, the first two equations become identical and can be reduced to one nonlinear diffusion equation [33]. This justifies using v_e from Eq. (5) as a natural scale for the entrainment velocity at the cooling stage.

In context of the reported study, Eq. (5) reduces to $v_e(t) = \beta(\delta T/R)$, where $\delta T = T - T_a$ is a characteristic temperature difference (e.g., averaged over thermal's volume; see below) and the ambient temperature $T_a = \text{const}$. It is worth mentioning that the scaling for entrainment velocity, $v_e \propto 1/R$, has been recently introduced in models of atmospheric thermals [25,26].

We found that the dynamics of strong thermals can be drastically different from weak Boussinesq thermals. In general, this evolution is affected by the interplay of two processes: (1) entrainment flux caused by thermal expansion, Eq. (5), and (2) solid-body acceleration of the thermal centroid (similar to acceleration of a rising bubble in fluid). As a result, scaling laws in Eqs. (1) and (2) are modified with different power-law exponents. The refined values of these exponents depend on the initial density contrast between the thermal and the ambient environment. They eventually approach the values predicted by the BMT model at the long-time limit, when the thermal dissipates its initial energy and becomes weak. In this regard the scaling laws correspond to the so-called intermediate asymptotics [34] that may occur during the initial phase of thermal evolution. We validated our derived scaling numerically as well as with the available simulation and experimental data and found a reasonable agreement [35].

II. MODEL OF STRONG THERMALS

The motion of a buoyant thermal is governed by conservation equations for mass, momentum, and thermal flux that follow from equations of fluid dynamics for convective flow [36]. For the general (non-Boussinesq) case the conservation equations take the form

$$\frac{d}{dt}\left(\frac{4}{3}\pi \rho R^3 \right) = 4\pi \rho_a v_e R^2, \tag{9}$$

$$\frac{d}{dt}\left(\frac{4}{3}\pi \rho_* w R^3 \right) = \frac{4}{3}\pi g(\rho_a - \rho)R^3 - \frac{\pi}{2} C_D \rho_a R^2 w^2, \tag{10}$$

$$\frac{dB}{dt} = 0. \tag{11}$$

Here $R \equiv R(t)$ is the radius of the thermal (for simplicity its shape is assumed spherical), $w \equiv w(t)$ is the vertical velocity of its centroid, $v_e \equiv v_e(t)$ is the entrainment velocity of the fluid from the ambient environment into the thermal, C_D is the drag coefficient (introduced to account for energy dissipation in the system), $\rho \equiv \rho(t)$ is the average density inside the thermal, $\rho_a = \text{const}$ is the ambient density, and $\rho_* \equiv \rho_*(t) = \rho + \rho_a/3$, where the term $\rho_a/3$ accounts for the effect of inertial forces [29,37]. Parameter B is the total buoyancy of the thermal given by the integral of density (temperature) deficit over the thermal volume

$$B = (4/3\pi)\alpha g T_a K R^3, \tag{12}$$

where $K \equiv K(t)$ is the relative density contrast between the thermal and the ambient environment given by

$$K = \rho_a/\rho - 1 = T/T_a - 1. \tag{13}$$

Parameter B is proportional to the total energy released in the environment and is conserved during the evolution of the buoyant thermal, $B = B_0 = \text{const}$. When the thermal entrains surrounding fluid, its density deficit decreases by dilution in proportion to its volume increase thus keeping the product $(K\,V)$ constant, where $V \equiv V(t)$ is the volume of the buoyant thermal [36]. Translation to the Boussinesq approximation corresponds to condition $\rho_* = (4/3)\rho$ on the left-hand side of Eq. (10).

The last ingredient of the conventional plume theory is the entrainment velocity, v_e. It is usually assumed that the entrainment velocity is proportional to the thermal's vertical velocity, Eq. (4).

In the presented study we propose the following two-term model for the entrainment velocity:

$$v_e = v_{e1} + v_{e2} = a(\rho/\rho_a)^{1/2} w + \beta(T - T_a)/R. \tag{14}$$

The first term of this equation, v_{e1}, comes directly from the original model, Eq. (4). The second term, v_{e2}, is deduced from the entrainment velocity driven by thermal flux, Eq. (5), where the term $\partial T(r,t)/\partial r$ can be approximated by $(T - T_a)/R$.

The ratio of the two terms in Eq. (14) can be estimated as

$$A = \frac{v_{e1}}{v_{e2}} = \frac{awR}{\beta(T - T_a)} \left(\frac{\rho}{\rho_a}\right)^{1/2}. \tag{15}$$

It can be seen that for small radii of the thermal, R, or a strong temperature contrast, $T - T_a$, the contribution of the second term in Eq. (5) can be dominant. As the thermal rises and cools, the first term becomes more important, and the thermal evolution transitions to the conventional Boussinesq regime. This will be also confirmed by a numerical solution shown below.

We use Eqs. (8) to (11) and (14) to model the evolution of strong thermals. Indeed, the assumption about the spherical shape of the thermal is only an approximation. It is known that the initial shape of the spherical density perturbation will be distorted during its vertical elevation transforming to an ellipsoidal domain containing a toroidal vortex [29]. The proposed scaling theory disregards this distortion assuming the scaling laws are defined for some effective parameters of the thermal, *viz.*, the position of its centroid and its effective radius.

Furthermore, we assume that the air parcel radius is much less than the height of a homogeneous atmosphere which allows us to ignore atmospheric stratification. The change in atmospheric temperature by altitude and the wind effect were also disregarded [1].

Equations (9)–(11) can be reduced to a nondimensional form

$$\frac{dy}{dt} = F_1(y), \quad y(t = 0) = 1, \tag{16}$$

$$\frac{dw}{dt} = F_2(w, F_1), \quad w(t = 0) = 0, \tag{17}$$

where

$$F_1(y) = \frac{3\,v_e}{R_0} \frac{(1 + K)^2}{1 + 2K}\, y^{2/3} \tag{18}$$

and

$$F_2(w, F_1) = \left[\frac{3gK}{1 + K} - \frac{9}{8}\frac{C_D}{R_0}\frac{w^2}{y^{1/3}} - \frac{w}{y}\left(9\frac{v_e}{R_0}y^{2/3} + F_1\right)\right]\frac{1 + K}{4 + K}. \tag{19}$$

R_0 is the initial radius of the buoyant thermal at the initial time $t = 0$, $y = (R/R_0)^3$, $K_0 = \rho_a/\rho_0 - 1$, and $K \equiv K_0/y = K_0(R_0/R)^3$.

According to [33] a temperature-dependent thermal diffusivity can be introduced in this model as

$$\beta(T) = \beta_0 (T/T_0)^{\nu} = \beta_0 (\rho_0/\rho)^{\nu}, \tag{20}$$

where β_0 is the thermal diffusivity at $t = 0$ and exponent ν is a constant. The value of $\nu = 0$ is the temperature-independent limit, $\nu = 1/2$ corresponds to an ideal gas, and $\nu = 5/2$ to plasma [38].

The equation for entrainment velocity, Eq. (14), can be reformulated using Eqs. (8), (12), and (13), $y = (R/R_0)^3$ and the temperature-dependent thermal diffusivity, Eq. (20):

$$v_e = v_{e1} + v_{e2} = aw\left(\frac{1}{1+K}\right)^{1/2} + Q\frac{(1+K)^{\nu}}{y^{4/3}}, \tag{21}$$

where

$$Q = \frac{\beta_0 T_a^{\nu+1} K_0}{R_0 T_0^{\nu}}. \tag{22}$$

Similarly, the ratio of entrainment velocity components in Eq. (15) can be rewritten as

$$A = \frac{v_{e1}}{v_{e2}} = \frac{a\, w\, y^{4/3}}{Q(1+K)^{1/2+\nu}}. \tag{23}$$

III. SCALING LAWS

Equations (8), (16), (17), and (21) form a closed system of equations that can be solved analytically and numerically. The main parameters that control the scaling laws are the relative density contrast, K, Eq. (13), and the ratio of entrainment velocity components, A, Eq. (23). The cases of $K \gg 1$ and $K \ll 1$ correspond to strong and weak thermals, respectively, while $A \gg 1$ and $A \ll 1$ describe the flow- and thermal-dominated entrainment, respectively.

For $K \ll 1$ Eqs. (18) and (19) reduce to

$$F_1(y) \approx 3\frac{v_e}{R_0} y^{2/3}, \tag{24}$$

$$F_2(w, F_1) \approx \frac{3}{4} gK - \frac{9}{32}\frac{C_D}{R_0}\frac{w^2}{y^{1/3}} - \frac{w}{y}F_1 \tag{25}$$

with $v_e \approx aw + Q/y^{4/3}$, Eq. (21). For the case $A \gg 1$ $v_e = aw$ and we recover $\gamma = \delta = 1/2$ and $\eta = \theta = 1/4$, Eq. (1), which corresponds to the conventional BMT scaling. By virtue of similar arguments we arrive at $\gamma = 4/5$, $\delta = 1/5$, $\eta = 3/10$, and $\theta = 1/5$ for $A \ll 1$ (see the Appendix for details).

For the regime of $K \gg 1$ Eqs. (18) and (19) change to

$$F_1(y) \approx \frac{3}{2}\frac{K_0}{R_0}\frac{v_e}{y^{1/3}}, \tag{26}$$

$$F_2(w, F_1) \approx 3g - \frac{9}{8}\frac{C_D}{R_0}\frac{w^2}{y^{1/3}} - \frac{w}{y}F_1 \tag{27}$$

with $v_e \approx a\, w/K^{1/2} + QK^{\nu}/y^{4/3}$, Eq. (21). Similar to the previous case we consider two limits, $A \ll 1$ and $A \gg 1$, and arrive at different values of exponents: $\gamma = 2$, $\delta = 1/8$, $\eta = 0$, and $\theta = 1/4$ for $A \ll 1$ and $\gamma = 2$, $\delta = 4/5$, $\eta = 0$, and $\theta = 1/5$ for $A \gg 1$.

Table I summarizes the scaling laws describing the evolution of buoyant thermals under different conditions defined by K and A. The first row in the Table I shows the well-established scaling originating from the BMT model and the remaining rows our derived scaling.

TABLE I. Scaling law exponents, Eq. (1), for different conditions of the buoyant thermal evolution derived analytically. Parameters K and A are defined in Eqs. (13) and (23), respectively. [‡]Without the drag force $\eta = 2/5$ and $\gamma = 7/5$. [†]Assuming constant thermal diffusivity ($\nu = 0$); for temperature-dependent thermal diffusivity $\theta = (2+\nu)/(8+3\nu)$ and $\delta = 1/(8+3\nu)$ [see Eq. (A18) in Appendix A for details].

Conditions	η	γ	θ	δ
$K \ll 1$ and $A \gg 1$	1/4	1/2	1/4	1/2
$K \ll 1$ and $A \ll 1$	3/10[‡]	4/5[‡]	1/5	1/5
$K \gg 1$ and $A \gg 1$	0	2	1/5	4/5
$K \gg 1$ and $A \ll 1$	0	2	1/4[†]	1/8[†]

IV. RESULTS AND DISCUSSION

Our analytical predictions summarized in Table I have been validated by numerical solutions and available experimental data.

First-order nonlinear ordinary differential equations, Eqs. (16) and (17), with the entrainment velocity given by Eq. (21), were solved via Runge-Kutta discretization with parameters from the range that supports different scaling laws (Table I). The following constants and parameters were used: $T_a = 278$ K, $p_a = 101.3$ kPa, $a = 0.25$ [13], $\alpha = 3.43$ 1/K [39], $C_D = 0.47$ (for a bubble at moderate velocities) [1,37], $\nu = 0$, and $\beta_0 = 4 \times 10^{-6}$ m^2/(s K) [40,41]. The numerical simulations shown in this section assumed $K_0 = 0.1$ for weak thermals and $K_0 = 344$ for strong thermals.

The continuous line ("1"; see the figure legend) in Fig. 2 displays the log-log plot of radius, $R(t)$ [Figs. 2(a) and 2(c)], and elevation, $Z(t)$ [Figs. 2(b) and 2(d)], of the transient behavior of the buoyant thermal. Weak thermal gradients, $K_0 \ll 1$ [Figs. 2(a) and 2(b)], lead to a scaling, $\delta = 1/5$ and $\gamma = 7/5$ (dashed line "2"), before it changes to the BMT regime (dotted line "3"). Assuming $K_0 \gg 1$ (strong thermal gradients) [Figs. 2(c) and 2(d)] three scaling regions have been observed. At low timescales, initially another new regime can be seen (dash-dotted line "2") before the scaling manifests the same behavior (dashed line "3") as for the weak thermals, $K_0 \ll 1$ [Figs. 2(a) and 2(b)]. This region (dash-dotted line "2") reveals a very small scaling for the radius of the buoyant thermal ($\delta = 1/8$) and an accelerated rise ($\gamma = 2$) similar to an accelerated bubble rise in a fluid. A BMT region (dotted line "4") is again observed as the last regime during the thermal's evolution. Figure 3 displays the extracted power law exponents for the temporal evolution of the elevation and radius calculated as a derivation of the log-log dependence. The thick lines represent the numerical solution, and the thin lines are guides to the eye that indicate the scaling values derived analytically. The results show the transition between the different scaling regions depending on the density contrast between the thermal and the ambient environment. The scaling $\gamma = 4/5$ in Table I is not shown in Figs. 2 and 3, but it can be calculated numerically by assuming $A \ll 1$. The plots of numerical solutions for $K \gg 1$ and $A \gg 1$ (not presented here) are also in agreement with the analytical prediction.

Figure 4 shows the numerical simulation of radius and elevation of the thermal as a function of the total buoyancy. Power laws have been calculated for two regions of the initial density contrast, $K_0 \ll 1$ and $K_0 \gg 1$ (indicated by the asymptotes). At large timescales (continuous line) irrespective of the initial density contrast, K_0, the scaling agrees with the BMT model. However, at short timescales (dashed line) our model revealed scaling regimes $\theta = 1/5$ and $\eta = 2/5$ for $K_0 \ll 1$ and $\theta = 1/4$ and $\eta = 0$ for $K_0 \gg 1$. The scaling $\eta = 3/10$ derived analytically for $K \ll 1$ (Table I) can also be seen in the numerical simulation by assuming $A \ll 1$ (not shown here). The plots of numerical simulation for $K \gg 1$ and $A \gg 1$ have also been omitted here, but they are also in agreement with the analytical predictions shown in Table I.

The presented scaling laws for the evolution of convective buoyant thermals have been validated by published data. Figs. 5 and 6 display the transient behavior of the elevation and/or radius of a thermal generated by a high-fidelity simulation with a total energy released equal to 3.6×10^{16} erg

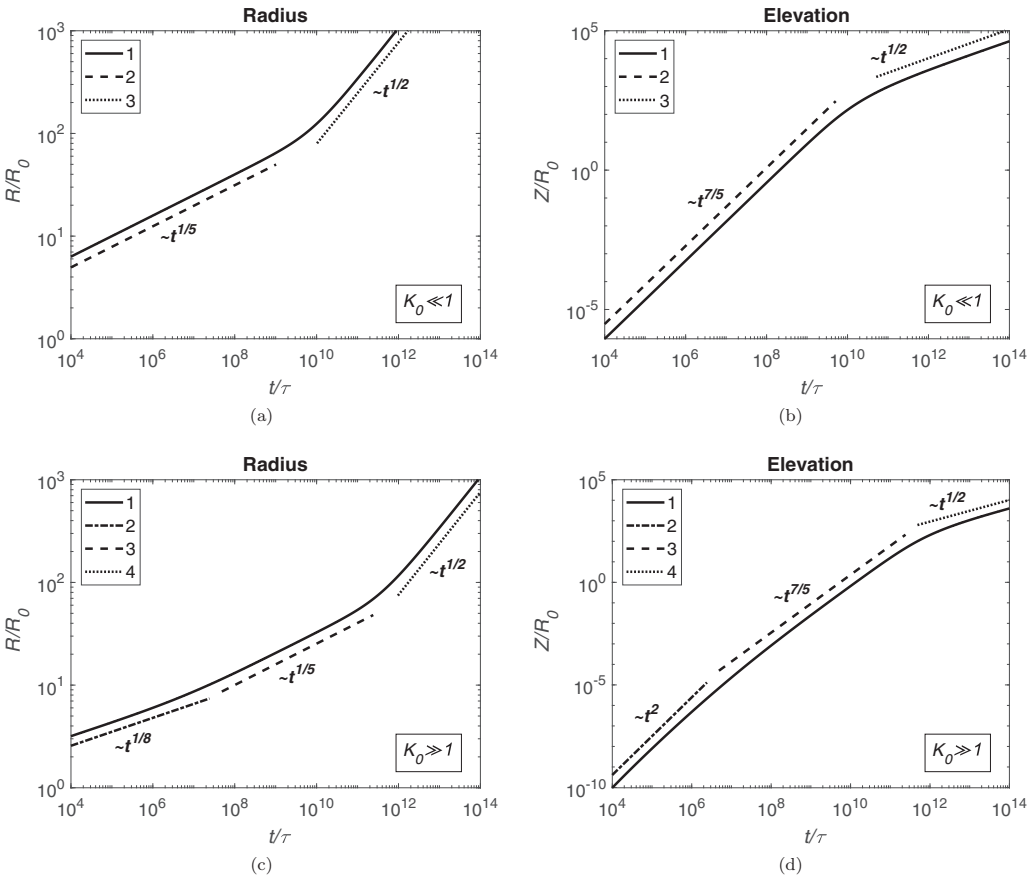

FIG. 2. Temporal dependency of the radius (a), (c) and elevation (b), (d) of a buoyant thermal in a log-log plot. The two top and two bottom graphs assumed an initial density contrast of $K_0 \ll 1$ and $K_0 \gg 1$, respectively. The lines on the plot are referred to also by numbers in the main text; see the legend.

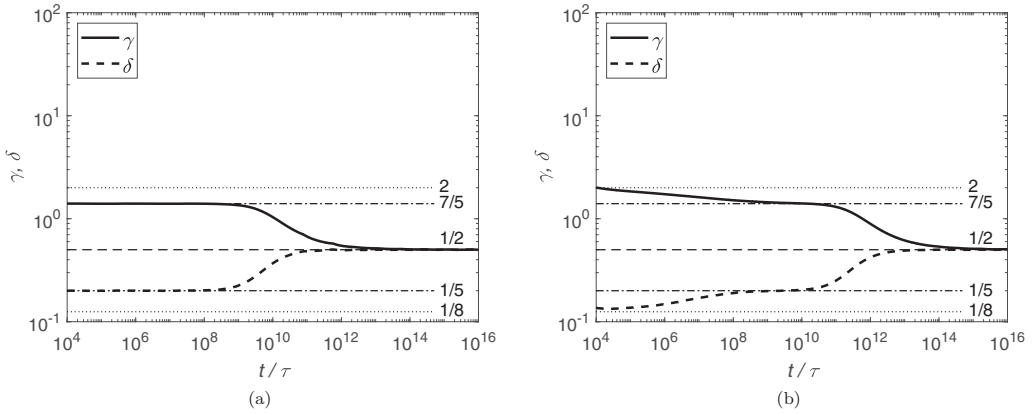

FIG. 3. Temporal dependency of power law exponents for elevation (γ) and radius (δ) of a buoyant thermal in a log-log plot for weak and strong thermal: (a) $K_0 \ll 1$, (b) $K_0 \gg 1$ [see Eq. (1)].

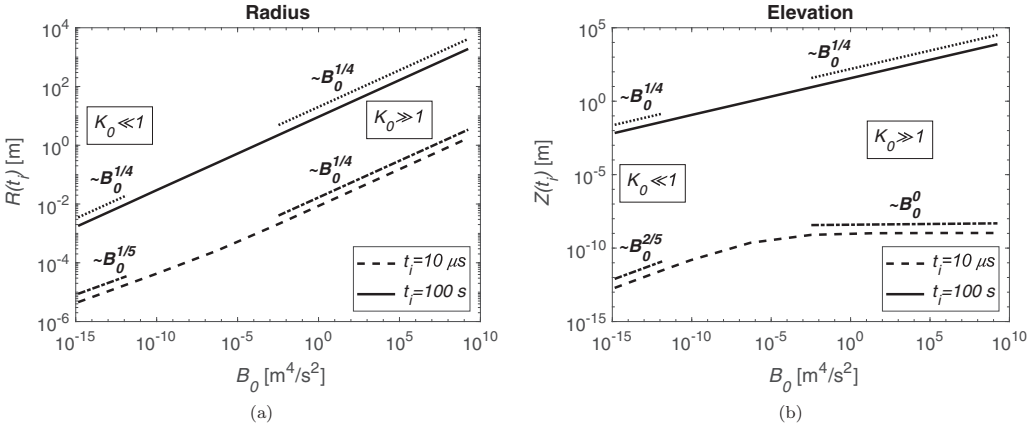

FIG. 4. Numerical simulation of the dependency of radius (a) and elevation (b) of the buoyant thermal on the total buoyancy. Two regions of the initial density contrast, $K_0 \ll 1$ and $K_0 \gg 1$, for short and large timescales are shown in a log-log plot.

[35] and experimentally by a nuclear explosion with an estimated yield of 8×10^{20} erg [42]. The open circles ("1") represent the published data, and the dashed line ("2") and the dotted line ("3") are a least-squares linear fit. The scaling exponents in the opposite limit of the extremely strong thermals (dashed line "2") confirm our derived scaling laws, $\delta = 1/5$ and $\gamma = 7/5$ (Fig. 5) and $\gamma = 4/5$ (Fig. 6) valid for weak thermals, $K \ll 1$. According to the presented model, a scaling of $4/5$ is observed when a drag force is included in the model and a scaling of $7/5$ without the drag force. Thus the experimental data set shown in Fig. 6 corresponds to the scenario with stronger drag than the data from [35] (Fig. 5). This can be due to the relatively large ratio of the energy released in the environment which is about 2×10^4. It is expected that stronger explosions would demonstrate a larger drag due to higher upward velocity [43].

The value of K_0 for the two data sets presented in Figs. 5 and 6 was estimated from the temperature T_0 and Eq. (13). For Fig. 5 $T_0 = 1500$ K and $T_a = 298$ K [35]. This leads to $K_0 \approx 4$. For the nuclear blast $T_0 \approx 150\,000$ K [30], and this leads to $K_0 \approx 500$. From these estimations it follows that Figs. 5 and 6 correspond to the cases $K_0 \approx 1$ and $K_0 \gg 1$, respectively.

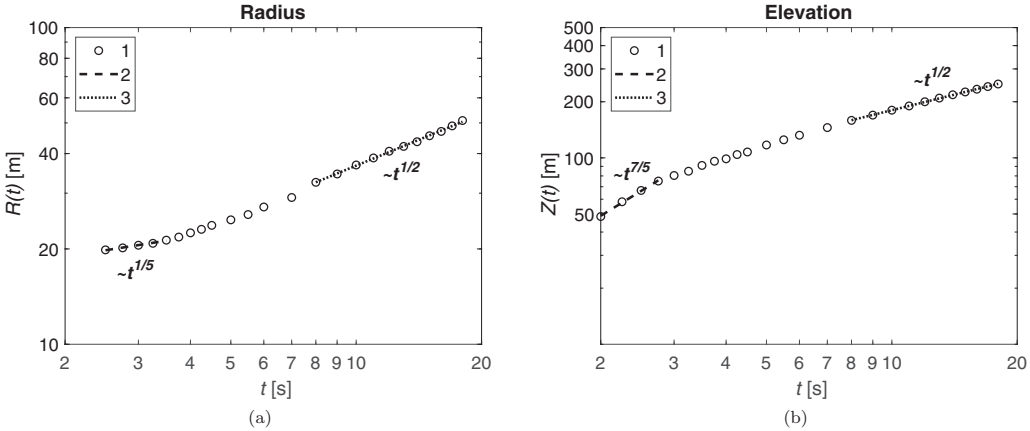

FIG. 5. Temporal evolution of the radius (a) and elevation (b) of a buoyant thermal in a log-log plot obtained by a simulation [35] and theoretical predictions, Eq. (1) and Table I. The lines on the plot are referred to also by numbers in the main text; see the legend.

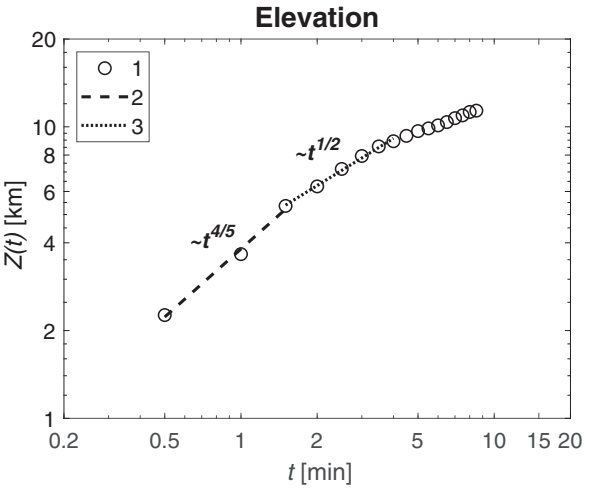

FIG. 6. Transient behavior of the elevation of a buoyant thermal in a log-log plot originating from an atmospheric nuclear test [42] and theoretical predictions, Eq. (1) and Table I. The lines on the plot are referred to also by numbers in the main text; see the legend.

The well-established BMT region has been also observed (dotted line "3"). The deceleration of the thermal at very high altitudes in Fig. 6 is due to the change of the surrounding atmosphere (density). This effect is outside of the scope of the present study [36]. Other examples of experimental data found in the literature revealed just the BMT scaling exponents, Eq. (2), most likely due to the lack of data availability at the early stage of the buoyant process [42–47].

V. CONCLUSIONS

To summarize, it has been shown that the evolution of convective thermals generated by a rapid energy release in the environment can exhibit a rich variety of scaling laws that cannot be explained by the conventional BMT model employing the Boussinesq approximation [11–13]. The presented study includes the extreme case when density inside the thermal is negligible in comparison with the environmental density. Our set of scaling laws, Eq. (1), with the value of exponents given in Table I have been derived and favorably validated with the limited data set available in the literature [35,42]. It is worth pointing out that these values are different from the values corresponding to ballistic motion of the thermal ($\gamma \approx 1$), and, as in the conventional BMT theory, cannot be explained as a simple compensation of drag with buoyancy, which is a typical scenario in atmospheric physics when entrainment fluxes can be disregarded [48].

Our scaling laws can also provide important insights into the scaling properties of strong convective turbulence (e.g., boiling fluid or solar atmosphere [49]). The latter can be conceptualized as a random ensemble of convective thermals [50], and this allows us to employ expressions in Eq. (1). Indeed, if we introduce scales of velocity components parallel and perpendicular to the horizontal boundary, $v_\perp \propto dZ/dt$ and $v_\parallel \propto dR/dt$, respectively, then from Eq. (1) we can arrive at the following relations:

$$v_\perp \propto B_0^{\eta/\gamma} Z^{1-1/\gamma}, \tag{28}$$

$$v_\parallel \propto B_0^{\theta+(\eta/\gamma)(1-\delta)} Z^{(\delta-1)/\gamma}. \tag{29}$$

The velocity components relate to Z being the distance from the underlying hot surface, which is also considered as the source of thermals. We observe that depending on regimes identified above (different values of γ, δ, η, and θ from Table I) this scaling is different.

One of the future options to extend these results is to map the gross parameters of an extremely strong thermal with the parameters of a toroidal vortex, in line with the conventional approach for the Boussinesq thermal [13,19,20]. This may provide interesting insights into the internal structure of extremely strong thermals and their long-term evolution.

We think that the presented results may be useful for understanding extreme events in the environment associated with generation of strong plumes and thermals (e.g., inferring their parameters from remote measurements) and validation of more complex numerical models.

APPENDIX: ANALYTICAL MODEL DERIVATION

The analysis below explores the different regimes of thermal evolution. Similar studies in the context of cloud evolution have been presented in [1,48].

1. Weak thermals ($K \ll 1$)

Under condition $K(t) \ll 1$ we obtain from Eqs. (18), (19), and (21) the following system of equations:

$$F_1(y) \approx 3\frac{v_e}{R_0}y^{2/3}, \tag{A1}$$

$$F_2(w, F_1) \approx \frac{3}{4}gK - \frac{9}{32}\frac{C_D}{R_0}\frac{w^2}{y^{1/3}} - \frac{w}{y}F_1, \tag{A2}$$

and

$$v_e = v_{e1} + v_{e2} \approx a\,w + \frac{Q}{y^{4/3}}. \tag{A3}$$

The function F_2, Eq. (A2), is the second-order polynomial of w. Initially, $F_2 \approx (3/4)gK$ since the rising velocity, w, is very small near $y = 1$. With increasing w, F_2 will eventually reach a point when $F_2 = 0$. This condition identifies two roots from which only one is positive

$$w = \frac{-v_{e2}}{2G} + \left[\frac{v_{e2}^2}{4G^2} + \frac{(gK_0/4)(R_0^3/R^2)}{G}\right]^{1/2}, \tag{A4}$$

where $G = (3C_D/32) + (v_{e1}/w)$, and v_{e1} and v_{e2} are defined in Eq. (A3).

The next step involved a simplification that employs different relative contributions of terms in Eq. (A3). We use Eq. (A4) for the estimation of the characteristic value of w. For $A \gg 1$ [see Eq. (23)], when the entrainment is controlled by the upward velocity, $v_e \approx v_{e1} \approx aw$, Eq. (A4) can be modified to

$$w \approx \left[\frac{(gK_0/4)(R_0^3/R^2)}{(3/32)C_D + a}\right]^{1/2}, \tag{A5}$$

and the solution of Eq. (16) with F_1 shown in Eq. (A1) leads to

$$R(t) = R_0(1 + t/\tau)^{1/2}, \tag{A6}$$

where $\tau = [R_0^2/(2a)][(\pi/2)(\alpha T_a C_D/B_0)]^{1/2}$. By assuming $t/\tau \gg 1$ and solving $w = dZ/dt$ with w from Eq. (A5) we arrive at

$$R(t) \propto B_0^{1/4}t^{1/2}, \tag{A7}$$

$$Z(t) \propto B_0^{1/4}t^{1/2}. \tag{A8}$$

Equations (A7) and (A8) are well-known scaling laws of the BMT theory [11–13].

For the case $A \ll 1$ the entrainment velocity is dominated by the thermal flux, $v_e \approx v_{e2} \approx Q/y^{4/3}$, the upward velocity in Eq. (A4) becomes

$$w \approx \frac{16}{3}\frac{QR_0^4}{C_D R^4}\left[-1+\left(1+\frac{3}{32}\frac{gC_D K_0 R^6}{Q^2 R_0^5}\right)^{1/2}\right], \tag{A9}$$

and the solution of Eq. (16) with F_1 from Eq. (A1) takes the form

$$R(t) = R_0(1+t/\tau)^{1/5}, \tag{A10}$$

where $\tau = R_0/(5Q)$. For $t/\tau \gg 1$, taking into account Eqs. (12) and (22) and solving $w = dZ/dt$ with w from Eq. (A9) we recover

$$R(t) \propto B_0^{1/5} t^{1/5}, \tag{A11}$$

$$Z(t) \propto B_0^{3/10} t^{4/5}. \tag{A12}$$

For the case with a negligible drag force applicable to short timescales when w is still small the scaling for the elevation will change to

$$Z(t) \propto B_0^{2/5} t^{7/5}, \tag{A13}$$

and the scaling for radius remains unchanged, Eq. (A11).

2. Strong thermals ($K \gg 1$)

Similar analysis can be conducted for the case of strong thermals, $K(t) \gg 1$. The original equations derived from Eqs. (18), (19), and (21) take the form

$$F_1(y) \approx \frac{3}{2}\frac{K_0}{R_0}\frac{v_e}{y^{1/3}}, \tag{A14}$$

$$F_2(w, F_1) \approx 3g - \frac{9}{8}\frac{C_D}{R_0}\frac{w^2}{y^{1/3}} - \frac{w}{y}F_1, \tag{A15}$$

and

$$v_e = v_{e1} + v_{e2} \approx a\, w\left(\frac{1}{K}\right)^{1/2} + Q\frac{K^\nu}{y^{4/3}}. \tag{A16}$$

For $A \ll 1$ when the entrainment is dominated by the thermal flux, $v_e \approx v_{e2} \approx QK^\nu/y^{4/3}$, the solution of Eq. (16) with F_1 displayed in Eq. (A14) yields

$$R(t) = R_0(1+t/\tau)^{1/(8+3\nu)}, \tag{A17}$$

where $\tau = [2/(8+3\nu)][R_0/(QK_0^{1+\nu})]$. By assuming $t/\tau \gg 1$, reformulating τ by taking into account Eqs. (12) and (22) and solving Eq. (17) with F_2 displayed in Eq. (A15) we derive scaling laws

$$R(t) \propto B_0^{(2+\nu)/(8+3\nu)} t^{1/(8+3\nu)}, \tag{A18}$$

$$Z(t) \propto t^2. \tag{A19}$$

Let's assume the case of the entrainment proportional to the upward velocity, $v_e \approx v_{e1} \approx awK^{-1/2}$ ($A \gg 1$), where w can be estimated from $F_2 = 0$,

$$w \approx \left(2\frac{g}{a}\frac{R_0}{K_0^{1/2}}\right)^{1/2} y^{5/12}. \tag{A20}$$

This regime occurs at a stage of the evolution of the thermal before the subsequent transition to the conventional BMT regime, Eqs. (A7) and (A8). Solving Eq. (16) with F_1 shown in Eq. (A14) leads to scaling

$$R(t) = R_0(1 + t/\tau)^{4/5}, \tag{A21}$$

where $\tau = (8/5)[R_0/(2ga)]^{1/2}K_0^{-1/4}$. Considering $t/\tau \gg 1$ and Eqs. (12) and (22) the radius of the buoyant thermal can be written as

$$R(t) \propto B_0^{1/5}t^{4/5}. \tag{A22}$$

The scaling laws for the elevation of the thermal remain the same as for the case of $A \ll 1$, Eq. (A19).

The values of exponents in Eqs. (A7), (A8), and (A11) to (A13), (A18), (A19), and (A22) correspond to the scaling laws observed at different regimes of the thermal evolution (weak and strong thermals, and the flow- and thermal-dominated entrainment). They are summarized in Table I.

[1] L. Chernogor, Dynamics of the convective rise of thermals in the atmosphere, Izv. Atmos. Ocean. Phys. **54**, 528 (2018).

[2] M. Cerminara, Modeling dispersed gas–particle turbulence in volcanic ash plumes, Ph.D. thesis, Scuola Normale Superiore, Pisa, Italy, 2016.

[3] G. Valsamos, M. Larcher, and F. Casadei, Beirut explosion 2020, A case study for a large-scale urban blast simulation, Safety Sci. **137**, 105190 (2021).

[4] L. David, Huge Meteor Explosion a Wake-Up Call for Planetary Defense, Sci. Am. **30**, 2 (2019).

[5] E. H. Anders, D. Lecoanet, and B. P. Brown, Entropy rain: Dilution and compression of thermals in stratified domains, Astrophys. J. **884**, 65 (2019).

[6] J. S. Turner, Jets and plumes with negative or reversing buoyancy, J. Fluid. Mech. **26**, 779 (1966).

[7] P. F. Linden, *Convection in the Environment. Perspectives in Fluid Dynamics: A Collective Introduction to Current Research* (Cambridge University Press, Cambridge, 2000).

[8] N. B. Kaye, Turbulent plumes in stratified environments: A review of recent work, Atmos. Ocean. **46**, 433 (2008).

[9] A. W. Woods, Turbulent plumes in nature, Annu. Rev. Fluid. Mech. **42**, 391 (2010).

[10] G. R. Hunt, Classical plume theory: 1337–2010 and beyond, IMA J. Appl. Math. **76**, 424 (2011).

[11] G. K. Batchelor, Heat convection and buoyancy effects in fluids, Q. J. Roy. Meteorol. Soc. **80**, 339 (1954).

[12] B. R. Morton, G. I. Taylor, and J. S. Turner, Turbulent gravitational convection from maintained and instantaneous sources, Proc. Roy. Soc. London A **234**, 1 (1956).

[13] J. S. Turner, Buoyant plumes and thermals, Ann. Rev. Fluid Mech. **1**, 29 (1969).

[14] R. A. Serway and R. J. Beichner, *Physics for Scientists and Engineers with Modern Physics*, 5th ed. (Saunders College Publishing, Fort Worth, Texas, 2000).

[15] Los Alamos National Laboratory, U. S. Department of Energy, Copyright ©2020, Triad National Security, LLC, All Rights Reserved, https://www.lanl.gov/discover/publications/national-security-science/2019-fall/mushroom-cloud-anatomy.php (December 2019).

[16] J. S. Turner, Buoyant vortex rings, Proc. R. Soc. Lond. A. **239**, 61 (1957).

[17] D. A. Haugen, *Lectures on Air Pollution and Environmental Impact Analyses* (American Meteorological Society, Boston, 1982).

[18] J. S. Turner, Turbulent entrainment: The development of the entrainment assumption, and its application to geophysical flows, J. Fluid. Mech. **173**, 431 (1986).
[19] A. C. H. Lai, B. Zhao, A. Wing-Keung Law, and E. E. Adams, A numerical and analytical study of the effect of aspect ratio on the behavior of a round thermal, Environ. Fluid. Mech. **15**, 85 (2014).
[20] B. Zhao, A. W. K. Law, A. C. H. Lai, and E. E. Adams, On the internal vorticity and density structures of miscible thermals, J. Fluid. Mech. **722**, R5 (2013).
[21] T. S. Van Den Bremen and G. R. Hunt, Universal solutions for Boussinesq and non-Boussinesq plumes, J. Fluid Mech. **644**, 165 (2010).
[22] G. Michaux and O. Vauquelin, Solutions for turbulent buoyant plumes rising from circular sources, Phys. Fluids. **20**, 066601 (2008).
[23] M. A. Delichatsios, Strong turbulent buoyant plumes. I. Similarity, Combust. Sci. Technol. **24**, 191 (1980).
[24] G. G. Rooney and P. F. Linden, Similarity considerations for non-Boussinesq plumes in an unstratified environment, J. Fluid Mech. **318**, 237 (1996).
[25] D. Lecoanet and N. Jeevanjee, Entrainment in resolved, dry thermals, J. Atmos. Sci. **76**, 3785 (2019).
[26] B. McKim, N. Jeevanjee, and D. Lecoanet, Buoyancy-driven entrainment in dry thermals, Q. J. R. Meteorol. Soc. **146**, 415 (2020).
[27] A. M. Blyth, A study of thermals in cumulus clouds, Q. J. R. Meteorol. Soc. **131**, 1171 (2005).
[28] J. Levine, Spherical vortex theory of bubble-like motion in cumulus clouds, J. Atmos. Sci. **16**, 653 (1959).
[29] N. Tarshish, N. Jeevanjee, and D. Lecoanet, Buoyant motion of a turbulent thermal, J. Atm. Sci. **75**, 3233 (2018).
[30] S. Glasstone and P. J. Dolan, *The Effects of Nuclear Weapons*, 3rd ed. (United States Department of Defense and United States Department of Energy, Washington, DC, 1977).
[31] X. Cao, G. Roy, P. Brousseu, L. Erhardt, and W. Andrews, A cloud rise model for dust and soot from high explosive detonations, Propelants Explos. Pyrotech. **36**, 303 (2011).
[32] E. E. Michaelides, Review-the transient equations of motion for particles, bubbles and droplets, J. Fluid. Eng. **119**, 233 (1997).
[33] B. Meerson, On the dynamics of strong temperature disturbances in the upper atmosphere of the Earth, Phys. Fluids **1**, 887 (1989).
[34] G. I. Barenblatt, *Scaling, Self-similarity, and Intermediate Asymptotics: Dimensional Analysis and Intermediate Asymptotics* (Cambridge University Press, Cambridge, 2009).
[35] D. Dobranic, D. A. Powers, and F. T. Harper, The fireball integrated code package, Sandia Report SAND97-1585, UC-505, Sandia National Laboratories (1997).
[36] B. Cushman-Roisin, *Environmental Fluid Mechanics* (Wiley-Blackwell, 2008).
[37] J. Magnaudet and D. Legendre, The viscous drag force on a spherical bubble with a time-dependent radius, Phys. Fluids **10**, 550 (1998).
[38] E. M. Lifshitz and L. P. Pitaevskii, *Physical Kinetics: Course of Theoretical Physics*, Vol. 10, Institute of Physical Problems, USSR Academy of Sciences, Moscow (Butterworth-Heinemann, 1981).
[39] Engineering ToolBox, Air-thermophysical properties, http://www.engineeringtoolbox.com/air-properties-d_156.html (2003).
[40] W. M. Rohsenow, J. P. Hartnett, and Y. I. Cho, editors, *Handbook of Heat Transfer*, 3rd ed. (McGraw-Hill Education, 1998).
[41] W. H. Heiser, D. T. Pratt, D. H. Daley, and U. B. Mehta, *Hypersonic Airbreathing Propulsion*, 5th ed. (American Institute of Aeronautics and Astronautics, 1994).
[42] T. Imanaka, Initial process of the nuclear explosion and cloud formation by the Hiroshima atomic bomb, IPSHU English Research Report Series Issue 28, Institute for Peace Science, Hiroshima University (2012), pp. 10–17.
[43] I. Yaar and A. Sharon, Calibration of a cloud rise for a Rdd scenario, in *Prevention, Detection and Response to Nuclear and Radiological Threats*, edited by S. Apikyan, D. Diamond, R. Way, NATO Science for Peace and Security Series (Springer, Dordrecht, 2008), pp. 193–205.
[44] J. V. Jodoin, Nuclear cloud rise and growth, Ph.D. thesis, Faculty of the Graduate School of Engineering and Management, Air Force Institute of Technology, Air University, Wright-Patterson AFB, Ohio, 1994.

[45] R. L. Basket and R. T. Cederwall, Sensitivity of numerical dispersion modeling to explosive source parameters, paper presented at the 84th Annual Meeting & Exhibition, Air and Waste Management Association, Vancouver, BC, Canada (1991).
[46] K. A. Sandman, Development of 2-dimensional cloud rise model to analyse initial nuclear cloud rise, Ph.D. thesis, Faculty of the Graduate School of Engineering and Management, Air Force Institute of Technology, Air University, Wright-Patterson AFB, Ohio, 2005.
[47] H. W. Church, Cloud rise from high-explosive detonations, Research Report SC-RR-68-903, Sandia Laboratories, Albuquerque, NM, 1969.
[48] D. M. Romps and A. B. Charn, Sticky thermals: Evidence for a dominant balance between buoyancy and drag in cloud updrafts, J. Atmos. Sci. **72**, 2890 (2015).
[49] A. Nordlund, R. F. Stein, and M. Asplund, Solar surface convection, Living Rev. Sol. Phys. **6**, 2 (2009).
[50] J. Werne, Plume model for the boundary-layer dynamics in hard turbulence, Phys. Rev. E **49**, 4072 (1994).